Genetic dissection of neuropeptide cell biology at high and low activity in a defined sensory neuron

Patrick Laurent[a,b,1], QueeLim Ch'ng[c], Maëlle Jospin[d], Changchun Chen[a], Ramiro Lorenzo[b], and Mario de Bono[a,1]

[a]Cell Biology Division, Medical Research Council Laboratory of Molecular Biology, Cambridge CB2 0QH, United Kingdom; [b]Laboratoire de Neurophysiologie, Université Libre de Bruxelles, 1050 Brussels, Belgium; [c]Centre for Developmental Neurobiology, Institute of Psychiatry, Psychology, and Neuroscience, King's College London, London SE1 1UL, United Kingdom; and [d]Institut NeuroMyoGène, Université Claude Bernard Lyon 1, 69100 Villeurbanne, France

Edited by H. Robert Horvitz, Massachusetts Institute of Technology, Cambridge, MA, and approved June 1, 2018 (received for review August 17, 2017)

Neuropeptides are ubiquitous modulators of behavior and physiology. They are packaged in specialized secretory organelles called dense core vesicles (DCVs) that are released upon neural stimulation. Unlike synaptic vesicles, which can be recycled and refilled close to release sites, DCVs must be replenished by de novo synthesis in the cell body. Here, we dissect DCV cell biology in vivo in a Caenorhabditis *elegans* sensory neuron whose tonic activity we can control using a natural stimulus. We express fluorescently tagged neuropeptides in the neuron and define parameters that describe their subcellular distribution. We measure these parameters at high and low neural activity in 187 mutants defective in proteins implicated in membrane traffic, neuroendocrine secretion, and neuronal or synaptic activity. Using unsupervised hierarchical clustering methods, we analyze these data and identify 62 groups of genes with similar mutant phenotypes. We explore the function of a subset of these groups. We recapitulate many previous findings, validating our paradigm. We uncover a large battery of proteins involved in recycling DCV membrane proteins, something hitherto poorly explored. We show that the unfolded protein response promotes DCV production, which may contribute to intertissue communication of stress. We also find evidence that different mechanisms of priming and exocytosis may operate at high and low neural activity. Our work provides a defined framework to study DCV biology at different neural activity levels.

neuropeptides | dense core vesicles | cell biology | secretory granules | membrane recycling

Stimulated neurons can release fast-acting neurotransmitters and slower-acting neuromodulators (1, 2). The largest and most diverse group of neuromodulators are the neuropeptides (3), which are ancient (4) and potent messengers that modulate most behaviors (5–10). Like neurotransmitters, neuropeptides are released following calcium (Ca^{2+}) entry, but whereas neurotransmitters are released from synaptic vesicles (SVs), neuropeptides are secreted from dense core vesicles (DCVs). DCVs contain an incompletely defined protein complement required to process, modify, and retain cargo peptides, and to traffic, dock, and release DCVs.

DCVs have distinct release properties from SVs (11, 12). They lack a local refilling mechanism and are replenished by de novo synthesis of neuropeptide precursors at the endoplasmic reticulum (ER). Neuropeptides are packaged into vesicles at the Golgi apparatus and trans-Golgi network, to mature into DCVs that are trafficked to release sites (13–15). DCVs have been studied most intensively in endocrine cells (16), which lack the long processes and synapses of neurons. Less is known about the mechanisms controlling DCV biogenesis, traffic, and release in neurons, about how DCV components are recycled, and about how these processes are influenced by physiological changes in neural activity.

Caenorhabditis elegans (*Ce*) has proved a useful model to study SVs (17). Mutants with defective traffic, loading, release, or recycling of SVs are viable and have highlighted conserved mechanisms (18–21). The nematode offers similar opportunities to study DCVs. *Ce* mutants with defective maturation of most neuropeptides have pleiotropic behavioral defects but are viable (22, 23). Importantly, the cell biology of DCVs can be studied in vivo in this transparent animal (24–29).

In this study, we establish a defined *Ce* neuron to study DCV biology. The neuron, called PQR, is an oxygen (O_2) sensor that forms en passant synapses along the ventral nerve cord. PQR is a tonic receptor whose activity can be set to "high" or "low" for long periods by altering ambient O_2 levels (30). PQR activity in vivo is largely independent of presynaptic input. We track and quantitate the in vivo fate of fluorescently tagged neuropeptides in active and inhibited PQR in hundreds of single- and double-mutant strains. Using unsupervised hierarchical clustering, we identify and study batteries of genes whose mutants show defects in DCV biogenesis, traffic, or release. We validate PQR as a model by confirming many findings previously made in multiple systems. We also highlight undescribed molecular functions, including a group of proteins that recycle DCV membrane proteins to newly maturing DCVs in the cell body.

Results

Cell Biology of DCVs in the PQR Neuron. We selected the PQR O_2 sensor as a defined neuron to study DCV cell biology in vivo because it is genetically tractable and its activity can by dialed up or down by changing the levels of its cognate stimulus, O_2 (30). PQR natively expresses multiple neuropeptides (31), and its dendrite, cell body, and axon lie in a single plane, facilitating imaging. PQR O_2-evoked Ca^{2+} responses were largely independent of presynaptic input and were not affected by mutations that

Significance

Neuropeptides are ubiquitous modulators of behavior and physiology. They are packaged in specialized secretory organelles called dense core vesicles (DCVs) that are released upon neural stimulation. Whereas local recycling of synaptic vesicles has been investigated intensively, there are few studies on recycling of DCV proteins. We set up a paradigm to study DCVs in a neuron whose activity we can control. We validate our model by confirming many previous observations on DCV cell biology. We identify a set of genes involved in recycling of DCV proteins. We also find evidence that different mechanisms of DCV priming and exocytosis may operate at high and low neural activity.

Author contributions: P.L. and M.d.B. designed research; P.L., M.J., C.C., and R.L. performed research; P.L., Q.C., and C.C. contributed new reagents/analytic tools; P.L., Q.C., M.J., R.L., and M.d.B. analyzed data; and P.L. and M.d.B. wrote the paper.

The authors declare no conflict of interest.

This article is a PNAS Direct Submission.

[1]To whom correspondence may be addressed. Email: patrick.laurent.ulb@gmail.com or debono@mrc-lmb.cam.ac.uk.

This article contains supporting information online at www.pnas.org/lookup/suppl/doi:10.1073/pnas.1714610115/-/DCSupplemental.

Published online June 29, 2018.

reduce synaptic vesicle exocytosis (*unc-13*) (19), DCV exocytosis (*unc-31*/*CAPS* Ca^{2+}-dependent activator protein for secretion) (24), or neuropeptide maturation (*egl-21*/*CPE*) (22, 23) (Fig. 1 *A* and *B*). These data suggest DCV mutant phenotypes in PQR are likely to be cell-autonomous.

To express transgenes selectively in PQR, we used the *gcy-32* promoter (32). Since promoter activity was an important variable for our assays, we compared the expression of a *pgcy-32::RFP* transgene at 21% O_2 across a panel of mutants, including *unc-64* (syntaxin), *unc-31* (CAPS), *unc-2* (P/Q voltage-gated Ca^{2+} channel), *gcy-35* (a soluble guanylate cyclase required for the O_2-evoked Ca^{2+} responses in PQR), and *unc-43* (CaMKII). We observed a small decrease in RFP expression in WD repeat and FYVE domain-containing 3 (*wdfy-3*) (see below) mutants, but unaltered expression in the other strains, suggesting the *gcy-32* promoter is relatively insensitive to changes in neuroendocrine signaling (Fig. 1*C*).

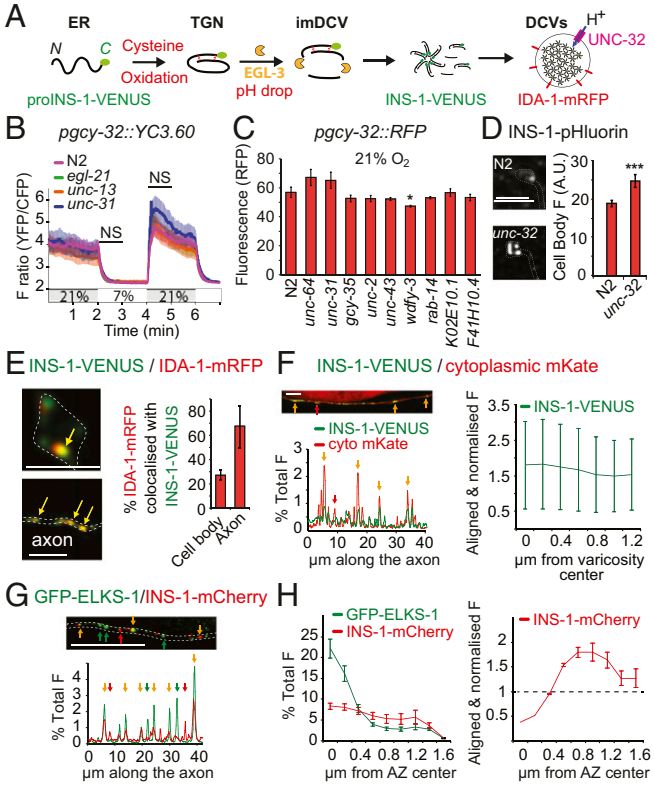

Fig. 1. DCVs in PQR. (*A*) Schematic showing maturation of prepro INS-1-VENUS. EGL-3/PC2, protein convertase 2; IDA-1/phogrin, a DCV membrane marker; imDCV, immature dense core vesicles. (*B*) Mutations affecting DCV (*unc-31*) or SV (*unc-13*) exocytosis, or neuropeptide processing (*egl-21*), do not alter O_2-evoked Ca^{2+} responses induced by 21% O_2 in PQR. n = 12–14. (*C*) Expression of a *pgcy-32::RFP* reporter is not modified by mutations that reduce PQR activity (*gcy-35*), exocytosis (*unc-2*, *unc-31*, *unc-43*, *unc-64*), or DCV biology (*rab-14*, *K02E10.1*, *F41H10.4*) at 21% O_2. One-way ANOVA followed by Tukey's post hoc test, n = 30–35. (*D*) INS-1-pHluorin is brighter in *unc-32* than N2 controls at 21% O_2; $n > 50$. *t* test. (*E*) Colocalization of INS-1-VENUS and IDA-1-mRFP (yellow arrows) in the cell body and axon of PQR at 21% O_2 (n = 13 and n = 10, respectively). (*F*) A representative axon shows peaks of cytoplasmic mKate fluorescence highlighting varicosities. The distribution of INS-1-VENUS fluorescence is aligned to the center of the enlargements and, when normalized for the cytoplasmic mKate fluorescence, showed no enrichment at varicosities (n = 5). (*G*) A representative axon shows INS-1-mCherry in proximity to the active zone marker GFP-ELKS at 21% O_2 (yellow arrow); INS-1-mCherry or GFP-ELKS only puncta can also be seen (red or green arrows, respectively). (*H*, *Left*) The distribution of INS-1-mCherry and GFP-ELKS-1 fluorescence aligned to the center of the GFP-ELKS-1 puncta. (*H*, *Right*) The distribution of INS-1-mCherry fluorescence normalized to the GFP-ELKS-1 fluorescence (n = 5). All bar graphs represent means ± SEM. For all statistical tests, *$P < 0.05$, **$P < 0.01$, ***$P < 0.001$. NS, not significant. (Scale bars: *D*, *F*, and *G*, 5 μm; *E*, 2.5 μm.)

Fluorescently tagged proneuropeptides have proven reliable reporters of DCV dynamics and neuropeptide secretion (24, 33, 34). To track neuropeptides and DCVs in PQR, we expressed human neuropeptide Y (NPY) tagged with RFP (NPY-RFP), and the *Ce* insulin-like peptide INS-1 tagged with VENUS (INS-1-VENUS). Like human proinsulin, INS-1 is predicted to comprise A and B chains processed from a propeptide by cleavage at dibasic residues, and held together by disulfide bonds (Fig. 1*A*). Previous work showed that a C-terminal GFP tag similar to ours remained attached to mature, oxidized INS-1 even after cleavage by EGL-3/PC2 (35). INS-1-VENUS and NPY-RFP localized to intracellular compartments in the PQR cell body and to puncta along the PQR axon, but were excluded from the dendrite. The two tagged peptides colocalized almost completely (*SI Appendix*, Fig. S1), suggesting they cosegregated to the same DCVs. In subsequent experiments, we used strains that express low levels of INS-1-VENUS from a low copy, integrated *pgcy-32::NS-1-VENUS* reporter transgene (*SI Appendix*, *Supplementary Methods*).

Neuropeptides are packaged in vesicles that become acidified as they mature into DCVs (13, 36, 37). We expressed INS-1 tagged with pHluorin in PQR to probe DCV acidification. pHluorin fluorescence is quenched below pH 5.5 (38). INS-1-pHluorin was faint and confined to the PQR cell body in wild-type animals (Fig. 1*D*). Disrupting *unc-32*, which encodes a conserved, neurally expressed vesicular proton pump subunit (39), increased INS-1-pHluorin fluorescence and revealed an INS-1-VENUS–like subcellular distribution. Thus, INS-1-pHluorin provides a readout of UNC-32–dependent DCV acidification.

To obtain further readouts of DCV biogenesis and maturation, we compared the distribution of INS-1-VENUS to that of a transmembrane protein that selectively labels DCVs, IDA-1/Phogrin (40, 41). In axons, 68% of INS-1-VENUS colocalized with IDA-1-mRFP, whereas in the cell body the two proteins showed only 27% colocalization (Fig. 1*E*). Thus, ∼75% of IDA-1 in the PQR cell body appears to reside in a compartment devoid of neuropeptides, possibly a recycling pathway (see below). For comparison, 95% of INS-1-VENUS in the axon, and 87% in the cell body, colocalized with NPY-RFP (*SI Appendix*, Fig. S1).

Axons are not uniform structures but harbor varicosities (42). To characterize INS-1-VENUS localization further, we correlated its fluorescence with a cytoplasmic marker, mKate (Fig. 1*F*). As expected, the two markers showed high correlation ($\rho = 0.640$, n = 7); however, after normalization to local cytoplasmic volume, INS-1-VENUS fluorescence was not found enriched in cytoplasmic enlargements. This suggests not all varicosities along PQR axon are presynaptic (Fig. 1*F*). Varicosities often but not always correspond to presynaptic sites (42).

Electron micrographs (EMs) show ∼15 presynaptic specializations distributed along the PQR axon in the ventral nerve cord (wormwiring.org/). EMs of *Ce* motor neurons suggest DCVs are excluded from within ∼150 nm of the active zone but are enriched perisynaptically close to the active zone (26, 43). We used the active zone marker GFP-ELKS-1 to locate presynaptic sites, which we defined as local maxima in this marker's fluorescence. In total, 50 ± 8% of INS-1-mCherry and 62 ± 8% GFP-ELKS-1 total fluorescence in the axon concentrated within 1.5 μm of presynaptic sites (34, 44, 45) (Fig. 1*G*). As expected, INS-1-mCherry did not colocalize with GFP-ELKS-1 ($\rho = 0.252$, n = 14) but is enriched around it. These observations are consistent with DCVs being enriched in the proximity of presynaptic sites in active PQR, as observed in EM studies of motor neurons. In summary, INS-1-mCherry/INS-1-VENUS fluorescence puncta likely correspond to DCVs enriched at perisynaptic regions.

NEUROSCIENCE

High-Dimension Analysis of DCV Distribution in PQR. We defined a set of parameters to describe the fate of INS-1-VENUS in PQR (Fig. 2 *A*–*C* and *SI Appendix*, *Supplementary Methods*). We measured INS-1-VENUS levels in the cell body as "cell body fluorescence" and calculated the fluorescence along the axon after background subtraction. We extracted the local maxima along the axon (Fig. 2*B*) and defined the mean of these "puncta" as "puncta fluorescence." The mean size of these puncta was quantified using the "full width at half-maximum (FWHM)" parameter, and the number of puncta per micrometer of axon with "puncta density per μm." We quantified the total fluorescence in the axon using the "area under the curve (AUC)" parameter. We also measured accumulation of fluorescence at the "tip of the dendrite" and at the "tip of the axon." Wild-type animals did not accumulate tagged neuropeptide at these locations, but some mutants did. We quantified these parameters using custom software from >60 images of PQR in animals kept at 21% O_2, or at 7% O_2 for 1 h, before image capture (Fig. 2 *C* and *D*). We also evaluated DCV exocytosis in animals kept at 21% O_2, using the established coelomocyte assay (44) (Fig. 2*E*). Coelomocytes are scavenger cells that endocytose molecules secreted in the pseudocoelomic cavity, including GFP-tagged neuropeptides. Posterior coelomocytes report the activity-regulated secretion of INS-1-VENUS from PQR and suggest INS-1-VENUS is released continuously at 21% O_2 (46). This release was significantly reduced in mutants defective in Ca^{2+}-regulated secretion such as *unc-64*/*syntaxin* and *unc-31*/CAPS (Fig. 2*E*).

Despite continuous release of INS-1-VENUS from PQR at 21% O_2, only a fraction of INS-1-VENUS redistributed intracellularly when we inhibited PQR activity by shifting animals to 7% O_2. By 2 h after this shift, cell body fluorescence had slightly but significantly increased, while the "total fluorescence" of the axon (AUC) was unchanged (Fig. 2*F*). This suggests a decrease in net DCV traffic from the cell body to the axon. The distribution of DCVs in the axon did, however, change: mean puncta fluorescence decreased, while puncta density increased (Fig. 2F). Thus, at low neuronal activity, DCVs spread into multiple smaller puncta instead of a few big puncta (Fig. 2*F*). The parameters we used allowed all puncta to be detected, both at 7% and 21% O_2. At both O_2 levels, most neuropeptide fluorescence remained in puncta: the ratio of mean puncta fluorescence to median axon fluorescence was not significantly altered by neuronal activity (Fig. 2*F*).

The absence of more drastic fluorescence changes suggests that DCV production in PQR is adjusted according to neuropeptide release, or that PQR releases only a small fraction of its DCV neuropeptide content.

Phenotypic Clustering of Mutants Reveals Functional Groups of Genes. We measured the parameters describing INS-1-VENUS fate in 187 mutant strains harboring defects in proteins with domains implicated in membrane traffic, neuroendocrine secretion, and neuronal or synaptic activity (Dataset S1). For each mutant we used the *t* statistic to compare parameter values with wild-type controls quantified in parallel (Fig. 2*D*). The *t* statistic scores differences between two groups, taking account of their variances and the sample size. The comparisons defined a phenotypic profile for each mutant. Our feature set allowed us to group mutants by profile similarity, using 24 nonsupervised hierarchical clustering methods that used bottom-up comparisons and could reach different conclusions from the same dataset. We used the most consensual of the clustering methods (uncentered correlation) to visualize the phenotypes and relatedness of mutants (Fig. 3 and *SI Appendix*, Fig. S2).

We were concerned that genetic modifiers in the background, an insufficiently large parameter set, and variability during feature extraction could yield false-positive or false-negative gene clusters. To minimize false positives, even at the expense of discounting genuine gene clusters, we set a conservative threshold. To be considered meaningful, gene groups had to be detected by >10 clustering methods. To test this threshold, we

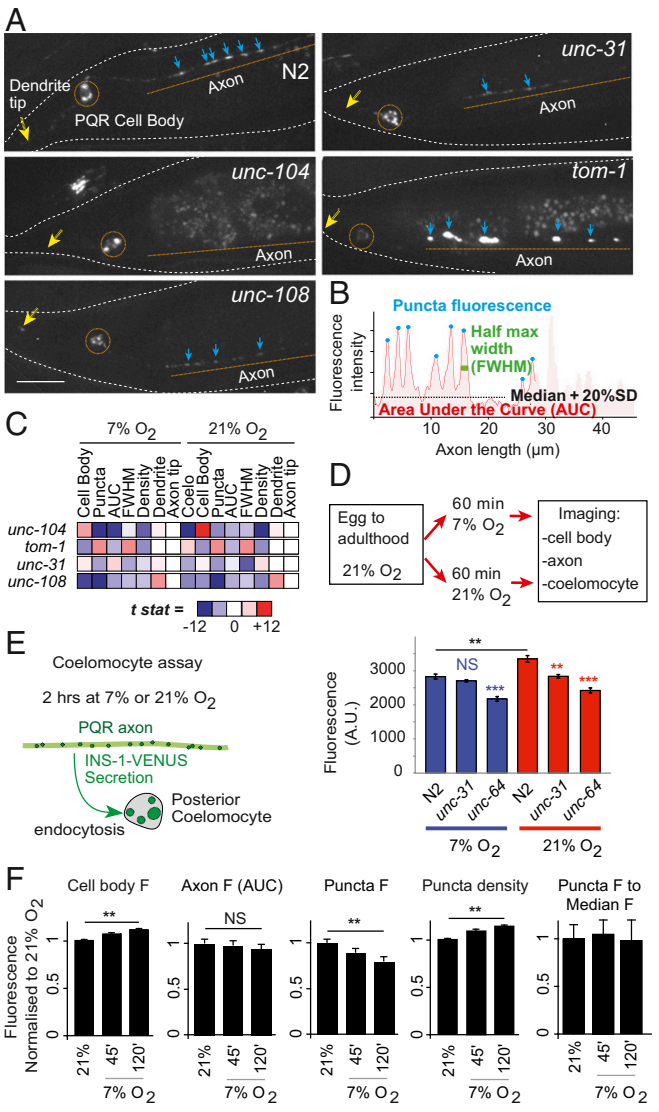

Fig. 2. Quantitative phenotyping. (*A*) The distribution of INS-1-VENUS in representative mutants at 21% O_2 highlights phenotypic differences that can be quantified. In all images, anterior is *Right* and posterior is *Left*. The PQR cell body (orange circle), axon (orange line), DCV puncta in the axon (blue arrows), and dendrite tip (yellow arrows) are indicated. (Scale bar: 5 μm.) (*B*) A scheme of the fluorescence trace along the axon showing the puncta parameters we quantified (for details, see *SI Appendix*). (*C*) For each parameter, we quantified the magnitude and significance of differences between mutant and wild-type controls using Student's *t* statistic. The *t* statistic $[t = \bar{x}_1 - \bar{x}_2/\sqrt{(S_1^2/n_1) + (S_2^2/n_2)}]$ is the ratio of the departure of the value of a parameter from the control to its SE. Shading intensity indicates the magnitude of the score, which ranges from −12 (max blue shading) to +12 (max red shading). *unc-31*, *unc-108*, *tom-1*, and *unc-104* mutant phenotypes are used as examples (n = 60–120 neurons). Axon tip showed no difference with the controls and are therefore displayed white. (*D*) Cultivation protocol: young adult worms were exposed for 1 h to 7% or 21% O_2 before imaging and quantification of 60–120 individuals. (*E*) The coelomocyte assay. INS-1-VENUS released from PQR is endocytosed by the coelomocyte, providing a proxy for PQR peptide secretion. Animals were grown at 21% O_2 and then exposed for 2 h to 7% or 21% O_2. All bar graphs represent means ± SEM; statistical significance: *t* test ($N > 60$). (*F*) Changes in fluorescence parameter values for animals grown at 21% O_2 and then exposed for 45 min or 2 h at 7% O_2. NS, not significant; $^{**}P < 0.01$, $^{***}P < 0.001$.

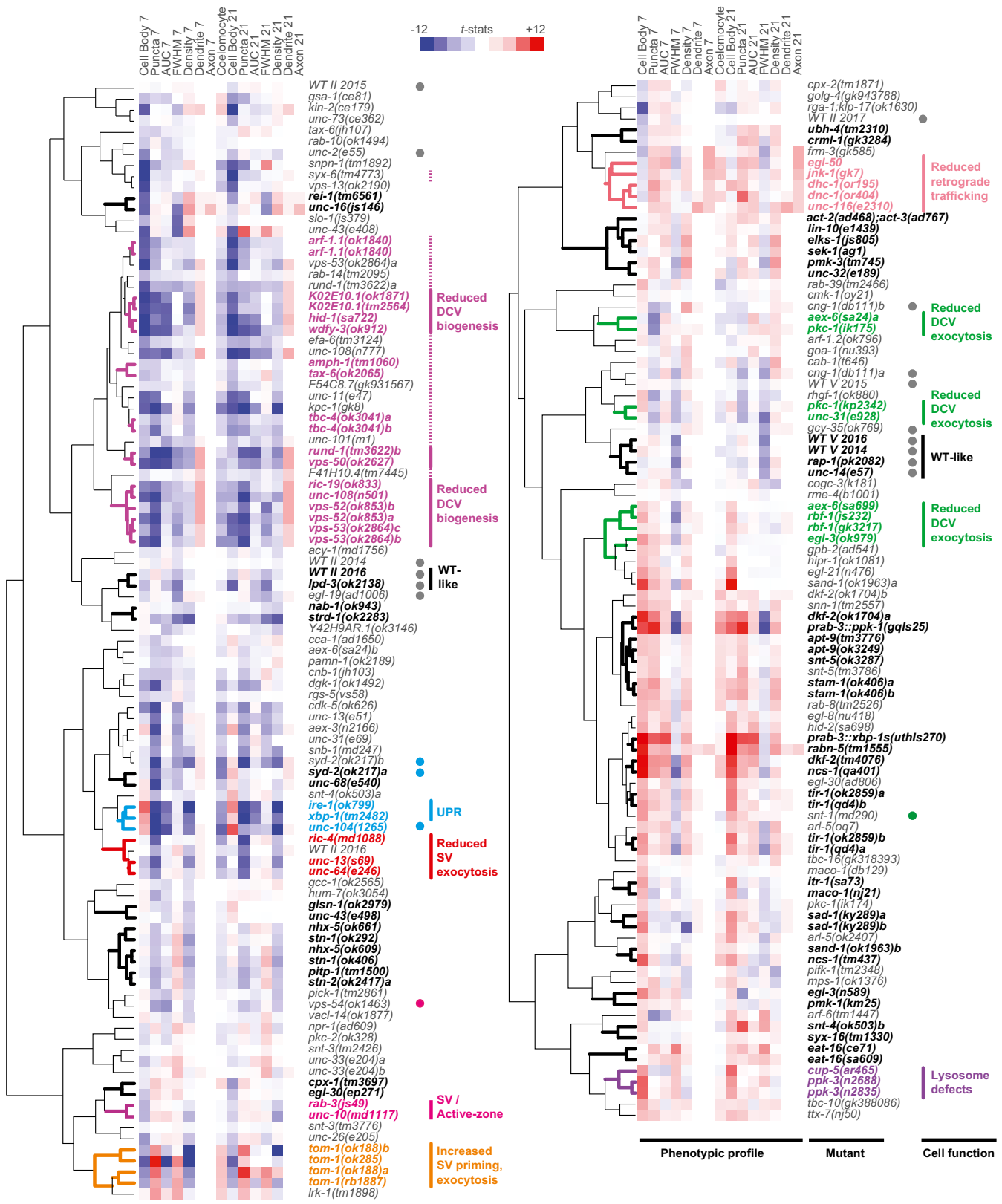

Fig. 3. Phenotypic clustering of mutants. The dataset is visualized using the uncentered correlation method. Each row represents the INS-1-VENUS distribution profile of one mutant strain. For each parameter, positive and negative *t* statistics (red and blue shading, respectively) indicate an increase or decrease, respectively, in a given parameter in the mutant compared with wild type. The magnitude of the *t* statistic (from −12 to +12) is indicated by the shading intensity. Bold branches in the dendrogram indicate robust clusters detected across ≥10 clustering methods. Colored lines indicate clusters with predicted functions that are indicated to the *Right*, based on the identity of genes included in the clusters. The control strains (here written WT II and WT V) are in the N2 genetic background and are compared with each other. The gray dots highlight mutants mentioned in the main text that have profiles similar to the wild-type controls. The other colored dots indicate genes of interest discussed in the main text.

included several independently derived strains bearing the same or different null alleles of the same gene. These strains should group together, whereas different, nonnull (hypomorphic and/or gain-of-function) alleles of the same gene are less likely to cluster. Forty-two percent of the positive controls (15/36 strain pairs bearing nulls) were clustered by >10 clustering methods; by contrast, none of six strain pairs bearing nonnull (loss- and/or gain-of-function) alleles were detected at this cutoff (*SI Appendix*, Fig. S2).

Using this threshold, we highlighted 62 groups containing two to six genes (Fig. 3, thick branches, and *SI Appendix*, Fig. S2). The fluorescence profile of mutants provided insights into processes affected by the mutation, while the clustering of mutant phenotypes predicted functionally related genes (34, 44, 47). To better anchor gene groups with biological function, we included in our dataset mutants characterized in previous behavioral, ultrastructural, or electrophysiological studies (Dataset S1). In the next several sections, we discuss gene groups highlighted by our clustering analysis.

A Baseline UPR Signaling Supports the Production of DCV. Our analysis clustered *ire-1* and *xbp-1* mutants (Fig. 3, cyan). In these animals INS-1-VENUS and the DCV membrane protein IDA-1/phogrin localized almost exclusively to the PQR cell body (Fig. 4*A*). IRE-1 and XBP-1 mediate the ER response to misfolded proteins by activating the unfolded protein response (UPR) (48). The UPR relieves ER stress by repressing general translation at the ER, while stimulating the ER's ability to fold, export, and degrade proteins. As expected if INS-1 traffic was blocked at the pH-neutral ER, INS-1-pHluorin fluorescence was higher in *xbp-1* mutants than wild-type controls and was excluded from the axon (Fig. 4*C*). Mutations that disrupt DCV biogenesis after ER exit, for example, *unc-104 kinesin* (40) or *hid-1* (see below) (49), did not alter the *xbp-1* phenotype (Fig. 4*B*). By contrast, VENUS targeted to the ER using a signal peptide was trafficked out of the cell body in *xbp-1* mutants. These data suggest a baseline UPR is required for efficient insulin export and DCV formation in PQR. Artificially increasing neuronal expression of XBP-1s, the isoform that induces the UPR, increased INS-1-VENUS/DCV production (Fig. 4*B*), suggesting the two processes are positively coupled.

Vesicles from the ER fuse with the *cis*-Golgi and their contents traffic to the trans-Golgi network (TGN). Neuropeptides exiting the TGN enter a short-lived, poorly characterized compartment commonly called immature dense core vesicles (imDCVs) (50). Apart from alleles that block ER exit or anterograde DCV movement (Fig. 3, cyan; see below), none of the mutants we tested, including double and triple mutants for the suggested neuropeptide sorting receptor *ida-1*/*phogrin* (51) and processing enzymes *egl-3*/*PC2*, *egl-21*/*CPE* showed the phenotype predicted for neuropeptide retention in the TGN, that is, increased INS-1-VENUS in the cell body and loss of INS-1-VENUS in axons (*SI Appendix*, Fig. S3 *A* and *B*). Although we cannot exclude a sorting-for-entry mechanism for neuropeptide traffic out of the TGN, the absence of mutants accumulating INS-1-VENUS in the TGN is more consistent with a sorting-by-retention model (52) in which INS-1-VENUS is retained in and/or retrieved to maturing DCVs, while proteins not destined for DCVs exit in vesicles budding off maturing DCVs.

A Large Group of Genes Involved in imDCV Maturation. Several mutants had phenotypes suggesting DCVs failed to retain peptide cargo as they matured: reduced INS-1-VENUS fluorescence in the cell body and axon of PQR, and in coelomocytes, both at 7% and 21% O_2 (Fig. 3, dashed magenta). We identified a group of 23 such genes clustered by eight or more methods. Included were eight genes recently shown to be involved in imDCV remodeling and cargo maintenance: *unc-108*/*Rab2*, *ric-19*/*ICA69*, *vps-50*, *vps-51*, *vps-52*, *vps-53*, *rund-1*, and *hid-1* (27, 29, 37, 53). Clustering with these eight genes were genes previously implicated in endosomal traffic and synaptic vesicle recycling, including *amph-1*/Amphyphysin, *syx-6*/Syntaxin6, *rab-4*/Rab14, *unc-11*/AP180, and *tax-6*/Calcineurin (54–56) (Fig. 3, dashed magenta). Also in the cluster were five genes not previously implicated in DCV biogenesis in any species: *K02E10.1*: a Rab related to RAB1/8/10; a Rab related to RAB-14; UNC-11: an ortholog of human AP180; *F41H10.4*: orthologous to human GRIPAP1 (also known as GRASP1) and *wdfy-3*, encoding a large protein conserved in humans that contains WD40 repeats, and FYVE and BEACH domains (Fig. 3, magenta). We observed a small decrease in expression from the *pgcy-32* promoter in *wdfy-3* mutants, but unaltered activity in the other strains (Fig. 1*C*).

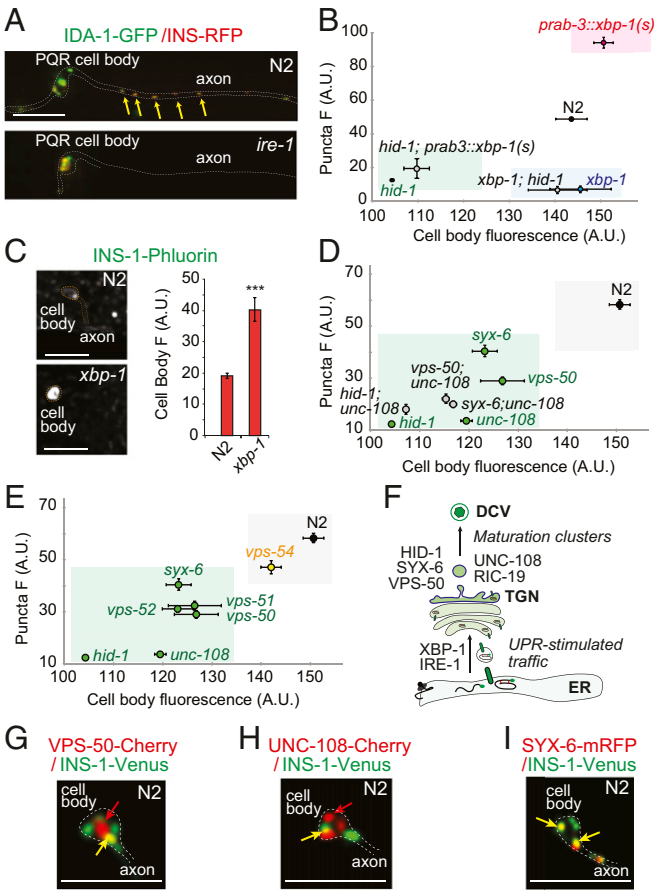

Fig. 4. (*A*) Disrupting *ire-1* prevents export of INS-1-VENUS and IDA-1-RFP from the PQR cell body. Arrows highlight DCVs in the axon. (*B*) The INS-1-VENUS phenotype of *xbp-1* mutants is not modified when DCV maturation is disrupted by loss of HID-1/Dymeclin (blue shading). Increasing XBP-1's expression strongly stimulates DCV production (magenta shading), which remains dependent on *hid-1* function (green shading). (*C*) INS-1-pHluorin is bright and retained in the cell body of *xbp-1* mutants compared with N2 controls, suggesting retention in the ER. (*D*) The distribution of INS-1-VENUS fluorescence in several mutants of the maturation clusters. Phenotypes of double mutants (green shading) suggest proteins of the maturation clusters are involved in the same cellular pathway. (*E*) Mutations disrupting the EARP complex (green shading) confer phenotypes distinct from those of a mutant lacking the GARP-specific *vps-54* subunit (gray shading). (*F*) Model. A baseline UPR-induced by XBP-1 signaling promotes exit of INS-1 and IDA-1 from the ER, allowing DCV production. UNC-108/Rab2, HID-1, SYX-6, and VPS-50 act after DCV acidification and INS-1 processing, but before a quality control step diverting imDCV cargo from the DCV. (*G–I*) The tagged EARP-specific subunit VPS-50-mCherry (*G*), Rab2/UNC-108-mCherry (*H*), and Syntaxin 6/SYX-6-mRFP (*I*) preferentially localize in the PQR cell body and proximal axon. Yellow arrows highlight the colocalized voxels; red arrows highlight mCherry or mRFP voxels. Bar graphs and scatterplots show means ± SEM. All experiments in the figure were performed at 21% O_2. (Scale bars: 5 μm.)

Double mutants of *unc-108* with *hid-1*, *syx-6*, or *vps-50* did not show additive phenotypes, suggesting genes in this cluster play related roles during DCV biogenesis (Fig. 4*D*). One proposed function of UNC-108/Rab2 and RIC-19 is to prevent loss of soluble imDCV cargo to endolysosomes (57). Previous work in *Ce* motoneurons showed that disrupting EGL-3/PC2 can partially prevent this leak in *unc-108* mutants (27). We found that disrupting *egl-3* rescued the INS-1-VENUS fluorescence phenotypes of *syx-6*, *hid-1*, *unc-101*, *rab-14*, *arf-1.1*, *unc-11*, and *vps-52* (*SI Appendix*, Fig. S3 *C* and *D*). This is consistent with these six genes regulating DCV biogenesis at a step after neuropeptides exit the TGN, when EGL-3/PC2 is activated by imDCV acidification. We therefore refer to the 23 clustering genes as the "maturation clusters." Consistent with a constitutive leak of neuropeptide from imDCV (28), several mutants that disrupt endocytic traffic toward lysosomes (*cup-5*/*mucolipin*, *ppk-3*/*Fab1p*, *vps-39*/*HOPS complex*, *sand-1*/*Mom1*) increased the INS-1-VENUS content in PQR. Mutations in *sand-1* and *vps-39* also improved the phenotype of *unc-108* (Fig. 3, purple, and *SI Appendix*, Fig. S3*A*).

The maturation clusters include proteins associated with the TGN and/or vesicles located near the TGN e.g., UNC-108/Rab2, RIC-19/ICA69, RUND-1/RUNDC1, HID-1/Dymeclin (27, 29). Other proteins in the maturation clusters are associated with recycling endosome compartments e.g., Syntaxin 6, RAB14, the EARP complex (made of VPS-50, 51, 52, and 53 subunits) and GRIPAP1 (58, 59). The EARP complex shares most of its subunits with the GARP complex, but includes the VPS-50 subunit, whereas GARP has VPS-54 (58). EARP mediates traffic toward the recycling endosome, whereas GARP promotes traffics toward the TGN. Disrupting VPS-50 but not VPS-54 perturbed INS-1-VENUS trafficking, consistent with recycling endosomes contributing to DCV biogenesis (53) (Fig. 3, magenta dot, and Fig. 4*E*). As expected (53), in PQR, mRFP-tagged VPS-50, UNC-108, and SYX-6 localized to the cell body, and to a lesser extent to the axon (Fig. 4 *G–I*). Together, these observations suggest recycling endosomes promote maturation of DCVs in close proximity to the TGN, but after scission of imDCVs from the TGN.

Maturation Clusters Promote Recycling of DCV Membrane Proteins. Previous work focused on retrieval of peptide cargo as DCVs mature (27, 28, 53). However, several proteins in the maturation clusters, including UNC-11/AP180 and amphiphysin, mediate clathrin-dependent recycling of SVs at synapses (55). Like SVs, DCVs harbor many membrane proteins, and at least some can also be recycled after release (60, 61). The physiological role of this process is uncertain, but might contribute to DCV biogenesis.

We speculated that a quality control mechanism matches peptidergic cargo load with available DCV membrane proteins during DCV maturation. In this model, endosomal recycling of DCV membrane proteins prevents the leak of DCV cargo observed in the maturation clusters mutants. Among the many DCV membrane proteins potentially recycled to imDCV through recycling endosomes, we focused on IDA-1/Phogrin and PAMN-1/PAM (peptidylglycine alpha- amidating monooxygenase), both specific markers for DCVs, and on the H^+/ATP pump required for DCV acidification. If genes in the maturation clusters promote recycling of DCV membrane proteins, their corresponding mutants should misroute DCV membrane proteins, reducing the colocalization of IDA-1, PAMN-1 and the H^+/ATP pump with INS-1. To test this we focused on the new genes we identified: *F41H10.4*, *wdfy-3*, or *K02E10.1*; and on *vps-50*, known to affect recycling toward recycling endosomes.

We first examined the distribution of IDA-1 and PAMN-1. In the cell body of wild-type PQR ~25% of IDA-1 and PAMN-1 colocalized with INS-1-VENUS. Disrupting *vps-50*, *F41H10.4*, *wdfy-3*, or *K02E10.1* reduced this colocalization to 5–15% (Fig. 5 *A* and *B*). Moreover, whereas ~65% of IDA-1 and PAMN-1 colocalized with INS-1-VENUS in wild-type axons, in mutants axon colocalization fell to 20–45%. These data suggest that in these mutants, recycling of DCV membrane proteins is disrupted before the recycling endosomes fuse with peptide-containing imDCV. Second, we monitored imDCVs acidification: if the vesicular H^+/ATP pump is not efficiently recycled to imDCVs, then INS-1-Phluorin fluorescence should increase in mutants of the maturation clusters. Consistent with this hypothesis, INS-1-pHluorin fluorescence increased significantly in *vps-50*, *hid-1*, *unc-108*, F41H10.4, *wdfy-3*, and *syx-6* mutants, but not in *ida-1* (Fig. 5*D*). If recycling endosomes are not fusing with peptide-containing imDCV in mutants of the maturation clusters, then these mutants might show an expanded recycling endosome compartment. To investigate this,

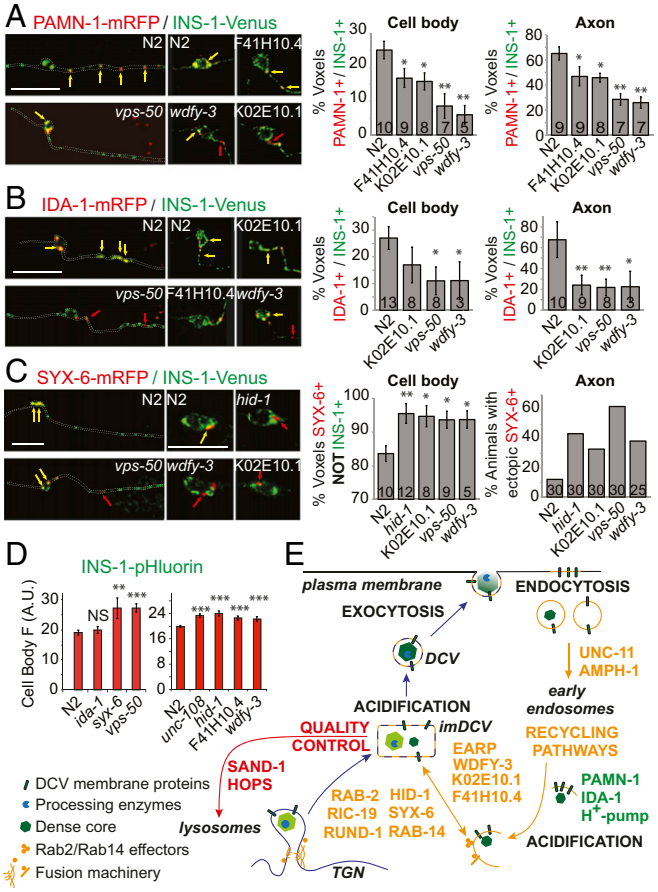

Fig. 5. Recycling of DCV membrane proteins. (*A*) Colocalization of INS-1-VENUS with PAMN-1-mRFP is reduced in mutants of the maturation cluster we tested. Yellow arrows highlight voxels showing colocalization; red arrows highlight mRFP-only voxels. (*B*) Colocalization of INS-1-VENUS with IDA-1-mRFP is also reduced in the maturation cluster mutants we tested. (*C*) The recycling endosome compartment that is SYX-6-mRFP (+)/INS-1-VENUS (–) expands in mutants of the maturation cluster. (*D*) INS-1-pHluorin fluorescence increases in mutants of the maturation cluster and in *syx-6*, but not in *ida-1* ($n > 50$). Note: Maturation cluster mutants have less INS-1-VENUS in their cell body than N2 controls (Fig. 4 *D* and *E*), so the histograms here likely underestimate the acidification defect. (*E*) Model: The protein products of the maturation clusters promote the recycling of DCV-membrane proteins, including IDA-1, PAMN-1, and the DCV proton pump. We postulate this recycling pathway intersects with DCV biogenesis post-TGN, and before the leak to endolysosomes, because the phenotype of these mutants is improved when endolysosomal trafficking is compromised, or when propeptide processing is disrupted. Moreover, *Drosophila* orthologs of many genes in the maturation clusters interact specifically with the endosomal Rabs RAB2, RAB4, and RAB14 (*SI Appendix*, Fig. S4). Bar graphs represent mean ± SEM. Statistics used one-way ANOVA followed by Tukey's post hoc test; $n = 5–13$. All experiments in the figure were performed at 21% O_2. (Scale bars: 5 μm.)

we quantified the SYX-6(+)/INS-1(−) compartment, likely reflecting recycling endosomes. In wild type, ~85% of SYX-6(+) vesicles did not contain INS-1; in *hid-1*, *vps-50*, *wdfy-3*, and K02E10.1 mutants, we observed a small but significant increase in this compartment (Fig. 5*C*). In sum, these data suggest that proteins in the maturation cluster promote recycling of DCV membrane proteins to imDCV through recycling endosomes (Fig. 5*E*).

Dynein Maintains the Mobility of DCVs. Two clusters with opposite phenotypes included genes encoding UNC-104/KINESIN 3 and SYD-2/LIPRIN-α on the one hand, and DHC-1/DYNEIN and UNC-116/KINESIN 1 on the other (Fig. 3, cyan and pink, and Fig. 6*A*). *unc-104*/kinesin three mutants showed increased INS-1-VENUS cell body fluorescence, and little or no fluorescence in the axon. Previous studies have shown that mutations in *unc-104*/kinesin 3 or *syd-2*/liprin-α disrupt anterograde traffic of several neural cargoes, including DCVs (40, 62, 63). SYD2 is suggested to activate UNC-104 (62). Consistent with this, *unc-104*; *syd-2* double mutants resembled *unc-104* single mutants (Fig. 6*A*).

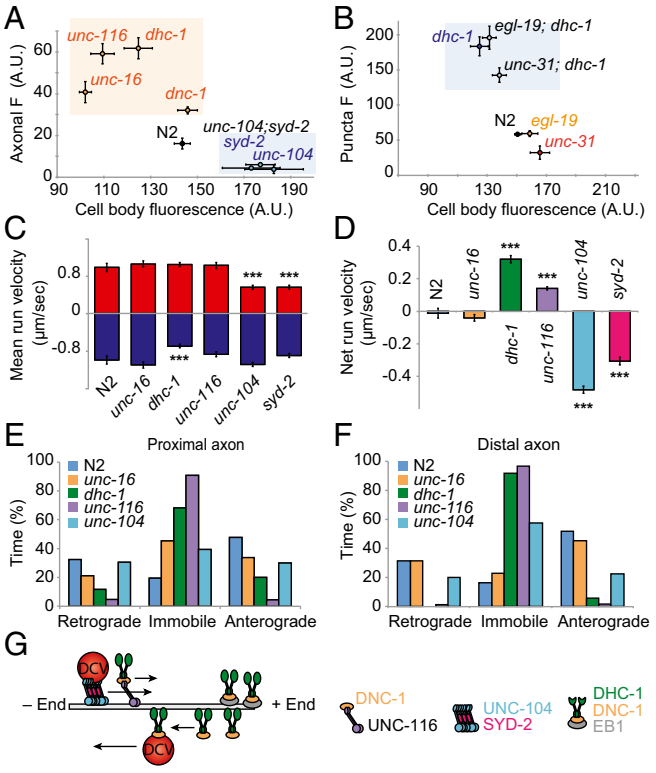

Fig. 6. DCV trafficking. (*A*) The distribution of INS-1-VENUS fluorescence in mutants for the dynein/dynactin motor complex (yellow shade), compared with mutants of the anterograde motor complex *unc-104* and *syd-2* (blue shade). The *unc-116* phenotype resembles that of *dhc-1 and dnc-1*. (*B*) The *dhc-1* phenotype is not modified by disrupting neuronal activity in *egl-19/L-VGCC* mutants, or reduced priming/exocytosis activity in *unc-31* mutants (blue shade). (*C*) Of the mutants studied, only *dhc-1* show significant defects in retrograde movement, whereas *unc-104* and *syd-2* both show reduced anterograde movement. (*D*) DCVs show net anterograde movement in *dhc-1* and *unc-116* mutants, and net retrograde movement in *unc-104* and *syd-2* mutants. (*E*) All mutants of the motor complexes show increased DCV immobility in the proximal axon. (*F*) In the distal axon, DCVs are often immobile in *dhc-1* and *unc-116* mutants. *unc-16* mutants resemble N2. (*G*) Model. UNC-116/Kinesin transports the dynein complex to the distal axon and improves bidirectional DCV trafficking. Bar graphs and scatterplots represent means ± SEM. Statistics are calculated using one-way ANOVA followed by Tukey's post hoc test, $n = 10–15$ movies/strains; >200 puncta. All experiments in the figure were performed at 21% O_2.

The second cluster showed the converse phenotype: reduced cell body fluorescence, but increased fluorescence in puncta and at the axonal tip. This cluster included *dhc-1* (dynein heavy chain), *dnc-1* (p150 subunit of dynactin), *unc-116* (kinesin-1 heavy chain), *jnk-1* (c-Jun kinase), and *egl-50* (Fig. 3, pink, and Fig. 6*A*). The *dhc-1* phenotype was not altered by reducing neuronal activity (in *egl-19* mutants lacking the L-type Ca^{2+} channel), or by disrupting priming/exocytosis in *unc-31* mutants (Fig. 6*B*), suggesting retrograde movement occurs independently of neuronal activity and DCV release. DCV accumulation along the PQR axon suggests dynein activity is required either to navigate DCVs around roadblocks along PQR axon microtubules or to prevent DCV accumulation at multiple microtubule plus ends along the PQR axon.

Kinesin-1 promotes anterograde trafficking, whereas dynein promotes retrograde trafficking. These motors can simultaneously associate with the same cargo (64). Interestingly, mutations in *dhc-1*/dynein and *unc-116*/kinesin-1 had similar DCV trafficking phenotypes. To investigate how dynein and kinesin-1 influence DCV transport more closely, we quantified INS-1-RFP trafficking in the ALM mechanosensory neuron. ALM processes run laterally, close to the cuticle, making them ideally suited for visualizing DCV trafficking. We measured the fraction of mobile puncta, as well as their directionality and run velocity, in the proximal and distal portions of the ALM axon. As expected from previous studies (40, 63), *unc-104* and *syd-2* mutants had few INS-1-VENUS puncta in the axon, and their anterograde run velocity was reduced (Fig. 6*D*). Only *unc-104*, *syd-2*, and *dhc-1* mutants affected the mean anterograde DCV run velocities, whereas only *dhc-1* affected the mean retrograde DCV run velocity (Fig. 6 *C* and *F*), suggesting these motors/adaptors are key to DCV fast trafficking.

Consistent with a mostly indirect effect of *unc-116*/Kinesin-1 on DCV trafficking, an *unc-116* mutation had no effect on DCV run velocities but affected the general movement pattern of DCVs. In both *dhc-1* and *unc-116* mutants, the net movement of DCV was anterograde, while many DCVs were immobile at the distal and, to a lesser extent, the proximal axon (Fig. 6 *D* and *E*). Kinesin-1 transports dynein anterogradely with the dynactin complex and is required to provide dynein to the distal axon (65). Our results and the accumulation of DCVs at the tip of the axon in PQR and ALM support a model in which dynein activity is limiting for the retrograde net movement of DCVs in the distal axon of *unc-116*, *dnc-1*, and *dhc-1* mutants. Therefore, the *dhc-1*–like phenotype of Kinesin-1 and Dynactin mutants in PQR may reflect defective anterograde transport of the dynein/dynactin complex by Kinesin-1 (Fig. 6*G*).

DCVs Production in PQR: A Homeostatic System. Toggling PQR activity by changing O_2 levels only weakly altered the INS-1-VENUS fluorescence content of PQR (Fig. 2*E*). Disrupting molecules that mediate O_2-evoked Ca^{2+} responses in PQR [the soluble guanylate cyclase *gcy-35*, the cGMP channel subunit *cng-1*, the ryanodine receptor *unc-68*, the L-type voltage-gated Ca^{2+} channel *egl-19* (30)] also had relatively weak effects on the total amount of INS-1-VENUS fluorescence in PQR (Fig. 3, gray dots). Similarly, mutations known strongly to disrupt SV/DCV exocytosis (*unc-13*$_{S/L}$, *unc-31*, others) had relatively weak effects on the total amount of INS-1-VENUS fluorescence in PQR (Fig. 3, green and red, and Fig. 7 *A* and *B*). These observations suggest that, despite tonic release of neuropeptides at 21% O_2, DCV production in PQR efficiently adapts to the need of the neuron. Nevertheless, *unc-13*, *unc-31*, and other priming and docking mutants changed DCV distribution in the axon (see bellow).

Differential Control of Neuropeptide Release at High and Low Neuronal Activity. EMs of *Ce* neuromuscular junctions show a small number of SVs and DCVs that touch the plasma membrane and are said to be docked there (26, 66). "Docking" is thought to involve a

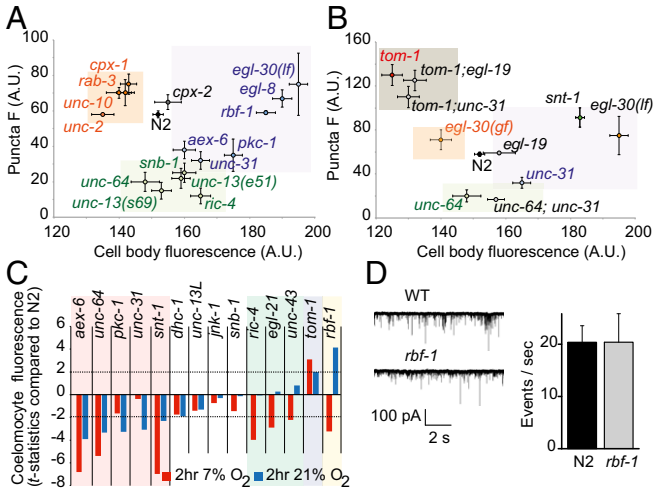

Fig. 7. DCV exocytosis. (*A*) Disrupting proteins that promote docking, priming, or exocytosis of DCVs (EGL-8/PLC; EGL-30/Gq; RBF-1/rabphilin) increased INS-1-VENUS fluorescence in the cell body but only weakly affected puncta fluorescence (purple shading). Disrupting proteins known to affect SV release reduced either the puncta fluorescence (green shading: UNC-64/Syntaxin; SNB-1/Synaptobrevin1a; RIC-4/SNAP25; UNC-13S/MUNC13Short) or the cell body fluorescence (orange shading: CPX-1/Complexin; UNC-10/RIM; UNC-2/P/Q-VGCC). All measurement made in animals kept at 21% O_2. (*B*) Disrupting *tom-1*/*tomosyn* strongly increased INS-1-VENUS puncta fluorescence. The effects of *tom-1* are independent of exocytosis and of elevated Ca^{2+}, as seen in double mutants with *unc-31*/*CAPS* and *egl-19*/*L-VGCC*, respectively (red shading). *egl-30*/G_q loss- and gain-of-function alleles show opposite phenotypes. All measurements were made in animals kept at 21% O_2. (*C*) Release of INS-1-VENUS induced by 21% O_2 is reduced in *unc-64*, *aex-6*, *pkc-1*, and *unc-31* mutants (orange shading). Release of INS-1-VENUS at 7% O_2 is reduced in *unc-64*, *aex-6*, *snt-1*, *ric-4*, *egl-21*, and *rbf-1*. Mutations in *tom-1* and *rbf-1* increase 21% O_2-induced release of INS-1-VENUS. The dashed line represents $P < 0.05$. (*D*) Loss of *rbf-1* does not alter the frequency of spontaneous EPSCs measured by electrophysiology at the neuromuscular junction. Bar graphs and scatterplots represent means ± SEM.

reversible interaction of vesicles with the plasma membrane before "priming," which leads to fusion in response to Ca^{2+} entry (67). For SVs, the proteins involved in these steps include the SNARE complex, formed by α-helices from syntaxin/UNC-64, SNAP25/RIC-4, and synaptobrevin/SNB-1, and the priming factors UNC-18, UNC-13, and UNC-31/CAPS, all previously characterized in *Ce* (24, 25, 68–72).

Several clusters contained these docking and priming factors: *unc-64* clustered with *unc-13(null)* and *ric-4*/*SNAP25; unc-31*/*CAPS* with *pkc-1*/protein kinase Cε, and *pkc-1* with *aex-6*/*Rab27* (Fig. 3, red and green). Although mutations in priming and docking factors had a weak effect on the total DCV content of PQR, they changed DCV distribution in the axon. In these mutants, INS-1-VENUS puncta fluorescence was reduced (Fig. 7*A*). In the same mutants INS-1-VENUS "AUC" weakly increased or remained unchanged (Fig. 3). This axonal phenotype suggests the perisynaptic distribution of DCVs was reduced due to spread or noncapture in *unc-64*, *unc-13*, *ric-4*, *pkc-1*, *aex-6*, and *unc-31* mutants. This could be explained by a lack of DCV docking sites, a less stable association with the plasma membrane (priming), or a change in the properties of the DCVs themselves.

Reciprocally, *tom-1* mutants, which disrupt Tomosyn, a presynaptic protein that inhibits docking, priming, and exocytosis of SVs and DCVs (73–75), showed increased puncta fluorescence (Fig. 3, orange). The *tom-1* phenotype was not altered when we disrupted the priming factor UNC-31, or the L-type voltage-gated Ca^{2+} channel α-subunit EGL-19, necessary for PQR depolarization (30) (Fig. 7*B*). This suggests Tomosyn can alter DCV docking independently of PQR activity and *unc-31*/CAPS function.

Synaptotagmin 1/SNT-1 triggers SV exocytosis in response to Ca^{2+} entry (76). *snt-1* mutants showed a weak increase in fluorescence in cell body and axonal parameters, regardless if animals were kept at 7% O_2 or 21% O_2 (Fig. 3, green dot, and Fig. 7*B*), suggesting SNT-1 promotes secretion of DCVs across the PQR activity levels we analyzed. To evaluate regulated exocytosis of DCVs in *snt-1* and other mutants, we used the coelomocyte assay (44) (Fig. 2*E*). Mutations in *aex-6*/*rab27*, *unc-64*, and *pkc-1* attenuated secretion both at 21% and 7% O_2, suggesting that they reduce docking, priming, and/or exocytosis of DCVs (Fig. 7*C*). In contrast, *tom-1* mutants showed increased coelomocyte fluorescence both at 7% O_2 and 21% O_2 (Fig. 7*C*). Disrupting *unc-31* and *snt-1* only reduced secretion at 21% O_2 and 7% O_2, respectively (Fig. 7*C*). Therefore, the functions of *unc-31* and *snt-1* appear more important at high and low neuronal activity, respectively. By comparison, *dhc-1* mutants, which also exhibited increased puncta fluorescence and provided a negative control, did not show a secretory phenotype (Fig. 7*C*). These data suggest different proteins may be involved in DCV exocytosis at high and low neural activity.

Specific Machineries Are Involved in SV or DCV Exocytosis. SVs are released at active zones, which contain several SV docking and priming factors including UNC-10 (RIM), RAB-3, CPX-1, and the UNC-13L long isoform that interacts with UNC-10 (19, 66, 77). As DCVs are excluded from the active zone and do not recycle locally, part of the SV machinery may not strongly influence DCV biology. Mutants *for unc-10*/*RIM1* and *rab-3* clustered together but showed a weak INS-1-VENUS phenotype compared with most mutants we studied (Fig. 3, pink, and Fig. 7*A*). This phenotype suggests these gene products either only have a weak direct effect on DCVs or that the reorganization of the SV cycle in mutants indirectly affects DCV cell biology. Interestingly, mutants selectively defective for UNC-13L, or for SNB-1, did not significantly reduce neuropeptide secretion (Fig. 7*C*), suggesting UNC-13L and SNB-1 affect SV release more strongly than DCV release (71, 78), at least in PQR.

Are some proteins involved in DCV but not SV exocytosis? Previous reports suggested that PKC-1 (*PKC epsilon*) and UNC-31 (*CAPS*) selectively affect DCV release (24, 25), although the selectivity of CAPS is controversial (79). These two mutants clustered with *aex-6*/RAB27 in our analysis (Fig. 3, green). Also clustering with *aex-6*/RAB27 mutants are two alleles of *rbf-1*, which disrupt a protein orthologous to Rabphilin that is present on DCVs (Fig. 3, green) (80). Like rabphilin, RBF-1 has two C2 domains and a FYVE domain. In the coelomocyte assay, *rbf-1* mutants showed an unusual secretion phenotype, with reduced secretion at 7% O_2 and increased secretion at 21% O_2, suggesting opposite effects in active and inactive neurons (Fig. 7*C*). To assess whether *rbf-1* selectively affected DCV exocytosis, or altered both SV and DCV exocytosis, we compared miniature excitatory postsynaptic potentials (mini-EPSPs) from *Ce* muscle in *rbf-1* mutants and wild-type controls. Spontaneous muscular mini-EPSPs reflect spontaneous release of SV at the neuromuscular junction and are affected by mutations in docking or priming factors for SV (81). Neither the frequency nor the size of mini-EPSPs was altered in *rbf-1* mutants, suggesting RBF-1 is not involved in SV release and may only affect DCVs in *Ce* neurons (Fig. 7*D*).

Discussion

We establish a tonic sensory neuron whose physiology we can control as a model to study DCV cell biology in vivo at high and low neural activity. We characterize DCV biogenesis, traffic, and release in 187 mutants that affect 143 genes. We focus our discussion on salient insights but note that we corroborate many observations made previously, validating PQR as a model.

NEUROSCIENCE

Efficient ER export of INS-1-VENUS and IDA-1-RFP requires a baseline UPR activity, and inducing the UPR increases DCV production. These observations suggest one mechanism by which altering the neuronal UPR could remodel intertissue communication (82).

We identify a set of gene products—located in the maturation clusters (Fig. 3)—that promote recycling of DCV membrane proteins, including IDA-1 and PAMN-1. Mutants of genes in the maturation clusters (*vps-50*, *hid-1*, *K02E10.1*, *F41H10.4*, *wdfy-3*, *syx-6*) fail to acidify DCVs appropriately and show reduced colocalization of DCV membrane proteins with neuropeptides. In the PQR cell body, ∼25% of IDA-1 and PAMN-1 colocalize with INS-1-VENUS in wild-type animals; this decreases to 10% in the maturation cluster mutants. We speculate that the IDA-1 and PAMN-1 not colocalized with INS-1 are in recycling compartments. In the axon of the maturation cluster mutants we studied, >60% of INS-1-VENUS is depleted of IDA-1, compared with <35% in wild type. These data suggest that a substantial fraction of IDA-1 is recycled rather than provided de novo by the TGN. These findings mirror results in the pancreatic beta-cell line Min6, which show that endogenous phogrin released after stimulation is recycled to an insulin-positive compartment and can be used during subsequent rounds of release (60). The molecular machinery mediating this recycling is unknown, but recycling phogrin is not observed to transit the TGN but transiently colocalizes with syntaxin-6 (60).

Several genes represented in the maturation clusters were implicated previously in DCV biogenesis. These include subunits of the recycling endosome (EARP) complex (37, 53, 58), UNC-108/Rab2, RIC-19, and HID-1 (49, 83). These studies highlighted roles for these genes in retrieving neuropeptides during DCV maturation, rather than in recycling DCV membrane proteins. Several other genes we identify in the maturation clusters were not previously associated with DCV biogenesis, including UNC-11/AP180, a protein involved in SV endocytosis at the plasma membrane (55); GRIPAP1, a tethering protein involved in endocytic recycling in neurons (59); WDFY3, a member of the BEACH protein family involved in cortical development (84); and Rab14 and RAB1/8/10. A large-scale screen for effectors of Rab small GTPases in *Drosophila* (85) found that orthologs of EARP, Rab-14, GRIPAP1, and WDFY-3 interact almost exclusively with Rab4, Rab14, or Rab2 (*SI Appendix*, Fig. S4). Rab4 and Rab14 act at the early "sorting" endosome, to assemble multiple classes of carrier vesicles, including recycling endosomes.

Altogether, the molecular identity of genes of the maturation clusters, the defect in DCV transmembrane protein recycling, and the expansion of the Syntaxin-6 positive compartment in some of the maturation clusters mutants support modifications to the current model for DCV biogenesis. We suggest the maturation cluster gene products function in recycling DCV transmembrane proteins from the plasma membrane back to the imDCV exiting the TGN. Evidence exists of post-TGN vesicular fusion events during DCV biogenesis in mammalian endocrine cells (86–88). These vesicular fusion events involve Syntaxin-6 and HID-1, both found in the maturation clusters (61, 87–89). These fusion events are described as "homotypic" because they occur between vesicles containing a dense-core, identified as imDCV. Instead, we suggest some of the observed homotypic fusion events involve recycling vesicles still containing a dense core after exocytosis and imDCVs exiting the TGN. Consistent with this, in lactotroph pituitary cells, many vesicles still containing prolactin after exocytosis colocalize transiently with internalized TfnR and Syntaxin-6, two markers of recycling endosomes (90). Therefore, DCV biogenesis is not a fully de novo process but involves a recycling trafficking pathway.

DCV content and distribution are relatively stable over short periods of PQR activity/inactivity (<1 h), despite evidence of constant neuropeptide release by the activated neuron. Moreover, mutants known to chronically reduce PQR activity, or SV and DCV release, showed relatively weak phenotypes. We recently showed that neurosecretion feeds back to increase neuropeptide transcription in tonically active neurons (46). We suggest production of DCVs is also coupled to neurosecretion through unknown feedback mechanisms. Increased availability of recycling endosomes containing DCV membrane proteins, following neurosecretion, may provide one such mechanism, by favoring retention of neuropeptides in maturing DCVs rather than their trafficking to lysosomes for degradation.

Disrupting proteins involved in DCV docking, priming, and exocytosis in PQR, reduces both the axonal puncta fluorescence and exocytosis in PQR; mutations that increase docking and priming have the opposite effect. These effects contrast with the effect of the same mutations on DCVs in motor neurons (44). However, it is consistent with their effects on SV redistribution in motor neurons (73). The differences between PQR and motor neurons might reflect dissimilar neuronal properties, or the non–cell-autonomous effects of the mutations on motor neuron activity. The DCV redistribution observed in docking-defective mutants is thought-provoking, since EM of the *Ce* neuromuscular junction reveals very few DCVs docked at the plasma membrane at steady state (26). Perhaps DCVs make transient and repeated interactions with the plasma membrane, whose duration/frequency would be determined by neuronal activity and the number of docking/priming sites.

Few genes affect SVs and DCVs differentially. Disrupting the active zone protein UNC-13L affects SVs without substantially altering DCVs in our assays, while RBF-1 (rabphilin) appears to affect only DCV biology.

In summary, our analysis provides a general way to identify and classify new, less well-described mutants with better understood ones. This procedure allowed us to identify and classify *K02E10.1*, *F41H10.4*, *wdfy-3*, and *syx-6* mutants, which were not described before. Based on their predicted function, we showed these genes and others in the maturation clusters are involved in DCV membrane protein recycling. Several other significant clusters were not explored here and will likely provide insights into DCV biology.

Methods

Two independent strains with integrated *[pgcy-32::ins-1(genomic)-VENUS::unc-54 3′UTR]* transgenes were crossed with 187 mutants strains listed in Dataset S1. Detailed methods are provided in *SI Appendix*, including cultivation procedure, quantitative imaging, and statistical analysis.

ACKNOWLEDGMENTS. We thank the Caenorhabditis Genetics Center (funded by NIH Infrastructure Program Grant P40 OD010440) and the Japanese Knockout Consortium for strains. We also thank Simon Bullock, Sean Munro, and members of the P.L. and M.d.B. laboratories for comments on the manuscript. This work was supported by fellowships from the Fondation Wiener Anspach and the European Molecular Biology Organization (to P.L.), and a grant from the Medical Research Council, United Kingdom (to M.d.B.).

1. Bartfai T, Iverfeldt K, Fisone G, Serfözö P (1988) Regulation of the release of coexisting neurotransmitters. *Annu Rev Pharmacol Toxicol* 28:285–310.
2. van den Pol AN (2012) Neuropeptide transmission in brain circuits. *Neuron* 76:98–115.
3. Fricker LD (2012) *Neuropeptides and Other Bioactive Peptides: From Discovery to Function*, Colloquium Series on Neuropeptides (Morgan and Claypool, San Rafael, CA).
4. Nikitin M (2015) Bioinformatic prediction of *Trichoplax adhaerens* regulatory peptides. *Gen Comp Endocrinol* 212:145–155.
5. Richter C, Woods IG, Schier AF (2014) Neuropeptidergic control of sleep and wakefulness. *Annu Rev Neurosci* 37:503–531.
6. Lutz PE, Kieffer BL (2013) Opioid receptors: Distinct roles in mood disorders. *Trends Neurosci* 36:195–206.
7. Bonnavion P, Mickelsen LE, Fujita A, de Lecea L, Jackson AC (2016) Hubs and spokes of the lateral hypothalamus: Cell types, circuits and behaviour. *J Physiol* 594:6443–6462.
8. White BH, Ewer J (2014) Neural and hormonal control of postecdysial behaviors in insects. *Annu Rev Entomol* 59:363–381.
9. Kim WJ, Jan LY, Jan YN (2013) A PDF/NPF neuropeptide signaling circuitry of male *Drosophila melanogaster* controls rival-induced prolonged mating. *Neuron* 80:1190–1205.
10. Anderson DJ (2016) Circuit modules linking internal states and social behaviour in flies and mice. *Nat Rev Neurosci* 17:692–704.

11. Moghadam PK, Jackson MB (2013) The functional significance of synaptotagmin diversity in neuroendocrine secretion. *Front Endocrinol (Lausanne)* 4:124.
12. van de Bospoort R, et al. (2012) Munc13 controls the location and efficiency of dense-core vesicle release in neurons. *J Cell Biol* 199:883–891.
13. Kim T, Gondré-Lewis MC, Arnaoutova I, Loh YP (2006) Dense-core secretory granule biogenesis. *Physiology (Bethesda)* 21:124–133.
14. Shakiryanova D, Tully A, Levitan ES (2006) Activity-dependent synaptic capture of transiting peptidergic vesicles. *Nat Neurosci* 9:896–900.
15. Wong MY, et al. (2012) Neuropeptide delivery to synapses by long-range vesicle circulation and sporadic capture. *Cell* 148:1029–1038.
16. Borgonovo B, Ouwendijk J, Solimena M (2006) Biogenesis of secretory granules. *Curr Opin Cell Biol* 18:365–370.
17. Barclay JW, Morgan A, Burgoyne RD (2012) Neurotransmitter release mechanisms studied in *Caenorhabditis elegans*. *Cell Calcium* 52:289–295.
18. McIntire SL, Reimer RJ, Schuske K, Edwards RH, Jorgensen EM (1997) Identification and characterization of the vesicular GABA transporter. *Nature* 389:870–876.
19. Richmond JE, Davis WS, Jorgensen EM (1999) UNC-13 is required for synaptic vesicle fusion in *C. elegans*. *Nat Neurosci* 2:959–964.
20. Jung N, et al. (2007) Molecular basis of synaptic vesicle cargo recognition by the endocytic sorting adaptor stonin 2. *J Cell Biol* 179:1497–1510.
21. Maeder CI, San-Miguel A, Wu EY, Lu H, Shen K (2014) In vivo neuron-wide analysis of synaptic vesicle precursor trafficking. *Traffic* 15:273–291.
22. Jacob TC, Kaplan JM (2003) The EGL-21 carboxypeptidase E facilitates acetylcholine release at *Caenorhabditis elegans* neuromuscular junctions. *J Neurosci* 23:2122–2130.
23. Husson SJ, et al. (2007) Impaired processing of FLP and NLP peptides in carboxypeptidase E (EGL-21)-deficient *Caenorhabditis elegans* as analyzed by mass spectrometry. *J Neurochem* 102:246–260.
24. Speese S, et al. (2007) UNC-31 (CAPS) is required for dense-core vesicle but not synaptic vesicle exocytosis in *Caenorhabditis elegans*. *J Neurosci* 27:6150–6162.
25. Sieburth D, Madison JM, Kaplan JM (2007) PKC-1 regulates secretion of neuropeptides. *Nat Neurosci* 10:49–57.
26. Hammarlund M, Watanabe S, Schuske K, Jorgensen EM (2008) CAPS and syntaxin dock dense core vesicles to the plasma membrane in neurons. *J Cell Biol* 180:483–491.
27. Sumakovic M, et al. (2009) UNC-108/RAB-2 and its effector RIC-19 are involved in dense core vesicle maturation in *Caenorhabditis elegans*. *J Cell Biol* 186:897–914.
28. Edwards SL, et al. (2009) Impaired dense core vesicle maturation in *Caenorhabditis elegans* mutants lacking Rab2. *J Cell Biol* 186:881–895.
29. Ailion M, et al. (2014) Two Rab2 interactors regulate dense-core vesicle maturation. *Neuron* 82:167–180.
30. Busch KE, et al. (2012) Tonic signaling from O_2 sensors sets neural circuit activity and behavioral state. *Nat Neurosci* 15:581–591.
31. Kim K, Li C (2004) Expression and regulation of an FMRFamide-related neuropeptide gene family in *Caenorhabditis elegans*. *J Comp Neurol* 475:540–550.
32. Yu S, Avery L, Baude E, Garbers DL (1997) Guanylyl cyclase expression in specific sensory neurons: A new family of chemosensory receptors. *Proc Natl Acad Sci USA* 94:3384–3387.
33. Rao S, Lang C, Levitan ES, Deitcher DL (2001) Visualization of neuropeptide expression, transport, and exocytosis in *Drosophila melanogaster*. *J Neurobiol* 49:159–172.
34. Ch'ng Q, Sieburth D, Kaplan JM (2008) Profiling synaptic proteins identifies regulators of insulin secretion and lifespan. *PLoS Genet* 4:e1000283.
35. Pierce SB, et al. (2001) Regulation of DAF-2 receptor signaling by human insulin and ins-1, a member of the unusually large and diverse *C. elegans* insulin gene family. *Genes Dev* 15:672–686.
36. Orci L, et al. (1987) Proteolytic maturation of insulin is a post-Golgi event which occurs in acidifying clathrin-coated secretory vesicles. *Cell* 49:865–868.
37. Paquin N, et al. (2016) The conserved VPS-50 protein functions in dense-core vesicle maturation and acidification and controls animal behavior. *Curr Biol* 26:862–871.
38. Kavalali ET, Jorgensen EM (2014) Visualizing presynaptic function. *Nat Neurosci* 17: 10–16.
39. Pujol N, Bonnerot C, Ewbank JJ, Kohara Y, Thierry-Mieg D (2001) The *Caenorhabditis elegans* unc-32 gene encodes alternative forms of a vacuolar ATPase a subunit. *J Biol Chem* 276:11913–11921.
40. Zahn TR, et al. (2004) Dense core vesicle dynamics in *Caenorhabditis elegans* neurons and the role of kinesin UNC-104. *Traffic* 5:544–559.
41. Torii S (2009) Expression and function of IA-2 family proteins, unique neuroendocrine-specific protein-tyrosine phosphatases. *Endocr J* 56:639–648.
42. White JG, Southgate E, Thomson JN, Brenner S (1986) The structure of the nervous system of the nematode *Caenorhabditis elegans*. *Philos Trans R Soc Lond B Biol Sci* 314:1–340.
43. Hoover CM, et al. (2014) A novel CaM kinase II pathway controls the location of neuropeptide release from *Caenorhabditis elegans* motor neurons. *Genetics* 196:745–765.
44. Sieburth D, et al. (2005) Systematic analysis of genes required for synapse structure and function. *Nature* 436:510–517.
45. Petzoldt AG, Lützkendorf J, Sigrist SJ (2016) Mechanisms controlling assembly and plasticity of presynaptic active zone scaffolds. *Curr Opin Neurobiol* 39:69–76.
46. Laurent P, et al. (2015) Decoding a neural circuit controlling global animal state in *C. elegans*. *eLife* 4:e04241.
47. Sönnichsen B, et al. (2005) Full-genome RNAi profiling of early embryogenesis in *Caenorhabditis elegans*. *Nature* 434:462–469.
48. Walter P, Ron D (2011) The unfolded protein response: From stress pathway to homeostatic regulation. *Science* 334:1081–1086.
49. Wang L, et al. (2011) HID-1 is a peripheral membrane protein primarily associated with the medial- and trans- Golgi apparatus. *Protein Cell* 2:74–85.
50. Tooze SA, Martens GJ, Huttner WB (2001) Secretory granule biogenesis: Rafting to the SNARE. *Trends Cell Biol* 11:116–122.
51. Saito N, et al. (2011) Luminal interaction of phogrin with carboxypeptidase E for effective targeting to secretory granules. *Traffic* 12:499–506.
52. Arvan P, Castle D (1998) Sorting and storage during secretory granule biogenesis: Looking backward and looking forward. *Biochem J* 332:593–610.
53. Topalidou I, et al. (2016) The EARP complex and its interactor EIPR-1 are required for cargo sorting to dense-core vesicles. *PLoS Genet* 12:e1006074.
54. McMahon HT, Boucrot E (2011) Molecular mechanism and physiological functions of clathrin-mediated endocytosis. *Nat Rev Mol Cell Biol* 12:517–533.
55. Rizzoli SO (2014) Synaptic vesicle recycling: Steps and principles. *EMBO J* 33:788–822.
56. Pavlos NJ, Jahn R (2011) Distinct yet overlapping roles of Rab GTPases on synaptic vesicles. *Small GTPases* 2:77–81.
57. Chun DK, McEwen JM, Burbea M, Kaplan JM (2008) UNC-108/Rab2 regulates post-endocytic trafficking in *Caenorhabditis elegans*. *Mol Biol Cell* 19:2682–2695.
58. Schindler C, Chen Y, Pu J, Guo X, Bonifacino JS (2015) EARP is a multisubunit tethering complex involved in endocytic recycling. *Nat Cell Biol* 17:639–650.
59. Hoogenraad CC, et al. (2010) Neuron specific Rab4 effector GRASP-1 coordinates membrane specialization and maturation of recycling endosomes. *PLoS Biol* 8:e1000283, and erratum (2010) 8:10.1371/annotation/b17dfb99-8809-4c5a-86c2-c2a0f7ca7f5e.
60. Vo YP, Hutton JC, Angleson JK (2004) Recycling of the dense-core vesicle membrane protein phogrin in Min6 beta-cells. *Biochem Biophys Res Commun* 324:1004–1010.
61. Wasmeier C, Burgos PV, Trudeau T, Davidson HW, Hutton JC (2005) An extended tyrosine-targeting motif for endocytosis and recycling of the dense-core vesicle membrane protein phogrin. *Traffic* 6:474–487.
62. Wagner OI, et al. (2009) Synaptic scaffolding protein SYD-2 clusters and activates kinesin-3 UNC-104 in *C. elegans*. *Proc Natl Acad Sci USA* 106:19605–19610.
63. Goodwin PR, Juo P (2013) The scaffolding protein SYD-2/Liprin-α regulates the mobility and polarized distribution of dense-core vesicles in *C. elegans* motor neurons. *PLoS One* 8:e54763.
64. Jolly AL, Gelfand VI (2011) Bidirectional intracellular transport: Utility and mechanism. *Biochem Soc Trans* 39:1126–1130.
65. Schuster M, et al. (2011) Controlled and stochastic retention concentrates dynein at microtubule ends to keep endosomes on track. *EMBO J* 30:652–664.
66. Weimer RM, et al. (2006) UNC-13 and UNC-10/rim localize synaptic vesicles to specific membrane domains. *J Neurosci* 26:8040–8047.
67. James DJ, Martin TF (2013) CAPS and Munc13: CATCHRs that SNARE vesicles. *Front Endocrinol (Lausanne)* 4:187.
68. Saifee O, Wei L, Nonet ML (1998) The *Caenorhabditis elegans* unc-64 locus encodes a syntaxin that interacts genetically with synaptobrevin. *Mol Biol Cell* 9:1235–1252.
69. Avery L, Bargmann CI, Horvitz HR (1993) The *Caenorhabditis elegans* unc-31 gene affects multiple nervous system-controlled functions. *Genetics* 134:455–464.
70. McEwen JM, Kaplan JM (2008) UNC-18 promotes both the anterograde trafficking and synaptic function of syntaxin. *Mol Biol Cell* 19:3836–3846.
71. Nonet ML, Saifee O, Zhao H, Rand JB, Wei L (1998) Synaptic transmission deficits in *Caenorhabditis elegans* synaptobrevin mutants. *J Neurosci* 18:70–80.
72. Richmond J (2005) Synaptic function. *WormBook,* 1–14.
73. Gracheva EO, et al. (2006) Tomosyn inhibits synaptic vesicle priming in *Caenorhabditis elegans*. *PLoS Biol* 4:e261.
74. Gracheva EO, et al. (2007) Tomosyn negatively regulates both synaptic transmitter and neuropeptide release at the *C. elegans* neuromuscular junction. *J Physiol* 585: 705–709.
75. Gracheva EO, Maryon EB, Berthelot-Grosjean M, Richmond JE (2010) Differential regulation of synaptic vesicle tethering and docking by UNC-18 and TOM-1. *Front Synaptic Neurosci* 2:141.
76. Nonet ML, Grundahl K, Meyer BJ, Rand JB (1993) Synaptic function is impaired but not eliminated in *C. elegans* mutants lacking synaptotagmin. *Cell* 73:1291–1305.
77. Koushika SP, et al. (2001) A post-docking role for active zone protein Rim. *Nat Neurosci* 4:997–1005.
78. Hu Z, Tong XJ, Kaplan JM (2013) UNC-13L, UNC-13S, and Tomosyn form a protein code for fast and slow neurotransmitter release in *Caenorhabditis elegans*. *eLife* 2: e00967.
79. Jockusch WJ, et al. (2007) CAPS-1 and CAPS-2 are essential synaptic vesicle priming proteins. *Cell* 131:796–808.
80. Mahoney TR, et al. (2006) Regulation of synaptic transmission by RAB-3 and RAB-27 in *Caenorhabditis elegans*. *Mol Biol Cell* 17:2617–2625.
81. Goodman MB, Lindsay TH, Lockery SR, Richmond JE (2012) Electrophysiological methods for *Caenorhabditis elegans* neurobiology. *Methods Cell Biol* 107:409–436.
82. Taylor RC, Dillin A (2013) XBP-1 is a cell-nonautonomous regulator of stress resistance and longevity. *Cell* 153:1435–1447.
83. Mesa R, et al. (2011) HID-1, a new component of the peptidergic signaling pathway. *Genetics* 187:467–483.
84. Orosco LA, et al. (2014) Loss of Wdfy3 in mice alters cerebral cortical neurogenesis reflecting aspects of the autism pathology. *Nat Commun* 5:4692.
85. Gillingham AK, Sinka R, Torres IL, Lilley KS, Munro S (2014) Toward a comprehensive map of the effectors of rab GTPases. *Dev Cell* 31:358–373.
86. Farquhar MG, Palade GE (1981) The Golgi apparatus (complex)—(1954–1981)—from artifact to center stage. *J Cell Biol* 91:77s–103s.
87. Urbé S, Page LJ, Tooze SA (1998) Homotypic fusion of immature secretory granules during maturation in a cell-free assay. *J Cell Biol* 143:1831–1844.
88. Du W, et al. (2016) HID-1 is required for homotypic fusion of immature secretory granules during maturation. *eLife* 5:e18134.
89. Wendler F, Tooze S (2001) Syntaxin 6: The promiscuous behaviour of a SNARE protein. *Traffic* 2:606–611.
90. Bauer RA, Overlease RL, Lieber JL, Angleson JK (2004) Retention and stimulus-dependent recycling of dense core vesicle content in neuroendocrine cells. *J Cell Sci* 117:2193–2202.